Accepted Manuscript

Tuning morphological features of lead iodide by low pressure vapor phase deposition

Alejandro Koffman-Frischknecht, Marcos Soldera, Flavio Soldera, Mauricio Troviano, Luciano Carlos, M. Dolores Perez, Kurt Taretto

Please cite this article as: Alejandro Koffman-Frischknecht, Marcos Soldera, Flavio Soldera, Mauricio Troviano, Luciano Carlos, M. Dolores Perez, Kurt Taretto , Tuning morphological features of lead iodide by low pressure vapor phase deposition. The address for the corresponding author was captured as affiliation for all authors. Please check if appropriate. Tsf(2017), doi:10.1016/j.tsf.2018.03.040

Tuning morphological features of lead iodide by low pressure vapor phase deposition

Alejandro Koffman-Frischknecht[a,b]*, Marcos Soldera[a,b], Flavio Soldera[c], Mauricio Troviano[a,b], Luciano Carlos[b], M. Dolores Perez[d] and Kurt Taretto[a,b]

[a]Departamento de Electrotecnia (FAIN-UNCo), Buenos Aires 1400, Neuquén, 8300, Argentina.

[b]Instituto de Investigación y Desarrollo en Ingeniería de Procesos, Biotecnología y Energías Alternativas (PROBIEN, CONICET-UNCo), Neuquén, 8300, Argentina.

[c]Department Materials Science and Engineering, Saarland University, Saarbrücken, D-66123, Germany.

[d]Departamento Energía Solar, GIyA - Instituto de Nanociencias y Nanotecnologías. Comisión Nacional de Energía Atómica (CNEA), San Martín, 1449, Argentina.

e-mail: alejandro.koffman@probien.gob.ar (A. Koffman-Frischknecht), telephone number: +54 299 4488305

*Corresponding author

Key words: perovskite solar cell precursors, low pressure vapor phase deposition, films growth

Abstract

Lead iodide (PbI_2) is a semiconductor with extensive use as an active layer for X-ray detectors and as a precursor for perovskite solar cells. Here we present a low vacuum method to obtain very uniform PbI_2 films with full substrate coverage. This method consists in the sublimation of PbI_2 inside a hot zone and its transport by an Ar flow to a substrate held at a controlled temperature. Using scanning electron microscopy combined with focused ion beam and X-ray diffraction we studied the morphology and crystallographic structure of the PbI_2 films with different deposition parameters: substrate and source evaporation temperature, deposition time and substrate material. At high substrate temperature (80ºC) and low evaporation temperature (310ºC) onto a glass sample, we obtained dense and smooth PbI_2 films showing hexagonal crystals, or platelets, stacked parallel to the substrate. The choice of the substrate material has a significant impact on the film morphology yielding porous-like structures with voids within the films for some substrates. A bandgap $E_g = 2.42$ eV and Urbach energy $E_U = 82.6$ meV were obtained by absorbance measurements, which are comparable to films

1

evaporated in high vacuum. Photoluminescence studies showed a dependence of the emission energies on the crystal orientation of the platelets which grow differently depending on the deposition conditions. The results show the ability of the low pressure vapor phase deposition technique to obtain good film properties, suitable for sensors and optoelectronic devices.

1 Introduction

Lead iodide is a wide-gap semiconductor with interesting electro-optical properties and as such, is widely used for X-ray detectors [1–3]. Recently, this material has received great attention as a precursor for obtaining metal organic perovskite solar cells [4–7]. In this technology, the main photoactive material is a perovskite with chemical formula ABX_3, where A is an organic molecule cation, B an inorganic cation like lead or tin and X the anion, which is a halogen element like iodide or chlorine. One of the most common perovskites is obtained from the reaction between lead iodide (PbI_2) and methylammonium iodide (MAI) that yields the metal organic perovskite $CH_3NH_3PbI_3$. Typically, this perovskite is obtained by exposing a previously deposited lead iodide film, to MAI from the liquid or vapor phase using a wide variety of techniques [8–10]. Some studies suggest that the morphology of PbI_2 film influences its reaction with MAI, e.g. it has been shown that unreacted PbI_2 remains for dense films, but a complete reaction can be achieved on porous PbI_2 films [11,12]. The MAI penetration is only a few nanometers deep for dense films [9,13,14], such that reaction is inhibited for thicker films.

A variety of deposition methods were used previously for lead iodide synthesis to obtain perovskite precursors [8–10], for applications in X-ray detectors or with the specific purpose to analyze the deposition and growth properties [15–17], including a carrier gas deposition method used to obtain lead iodide 2D nanosheets [18]. Each of these methods has interesting and unique characteristics for lead iodide processing, although they reveal shortcomings regarding the simultaneous accomplishment of fundamental features for large scale production of high quality films, such as low initial investment and low maintenance costs,

2

low material consumption, morphology tuning potential, high reproducibility and one-step processing capability, i.e. no need for post-deposition treatments.

Here we use the low pressure vapor phase deposition (LP-VPD) method, which is based on the organic vapor phase deposition (OVPD) concept developed since the mid-90s to fabricate organic solar cells and organic LEDs [19,20]. This method relies on the sublimation of a compound and its transport by an inert carrier gas towards a cooler zone where a substrate is located. The process takes place inside a low vacuum chamber heated externally with a four zone gradient, which prevents the back diffusion of the sublimed species. Along the vapor path towards the substrate, the temperature of the chamber is kept higher than the compound sublimation temperature in order to avoid condensation on the chamber walls. This feature maximizes material usage, offering a great advantage compared to conventional evaporation methods, such as vacuum thermal evaporation (VTE). Another benefit of this technique, in contrast with other gas carrier evaporation methods [18], is the possibility of fine tuning of the film morphology by adjusting the deposition parameters such as the substrate temperature, the back pressure, and the evaporation rate, which can be controlled by adjusting the source boat temperature and carrier gas flow [21,22]. We stress that this method is suitable for large substrate manufacturing [23,24] because it is in principle able to meet industrial standards such as efficient material usage, low chamber cleaning time, and low initial investment cost due to the low vacuum system components.

In this work, the LP-VPD method is employed to prepare lead iodide films on different substrates. This preparation technique allows us to study the tuning capability of lead iodide structural and morphological characteristics, by controlling simple parameters such us substrate temperature, evaporation temperature and deposition time. We use different substrates such as glass, indium tin oxide (ITO), fluorine doped tin oxide (FTO) and fluorine doped tin oxide coated with titanium dioxide (TiO_2). The selection of substrates used in this work is based on its potential use as electrodes for perovskite solar cells [25–27], X-ray

3

detectors [28], or on its use as substrate for optoelectronic characterization [17,29,30]. Structural and morphological properties are studied by X-ray diffraction (XRD) and scanning electron microscopy (SEM) combined with focused ion beam (FIB) to obtain cross section views. Reflectance-transmittance measurements in the visible spectrum are performed on PbI_2 films grown on quartz, to obtain the absorption coefficient, the optical band gap E_g and the Urbach energy E_U, yielding comparable results to those obtained in PbI_2 films prepared by high vacuum evaporation [31]. The interpretation of room temperature photoluminescence signal from PbI_2 films is also presented.

2   Experimental details

2.1   LP-VPD setup

Our low pressure vapor phase deposition system was designed and built in-house. The design of this system meets the needs of being compact, use of low-cost components and materials, and versatility to deposit different compounds. Fig. 1 (top) shows schematically the main components of the system and (bottom) the temperature profile used in all the depositions and the compound sublimation temperature ($T_{sublimation} \approx 300ºC$). The chamber is a 50 cm long and 5 cm diameter borosilicate glass tube. A rotary vane pump is used to generate a vacuum up to 0.1 mbar inside the chamber, which is measured with a digital Pirani gauge. The glass chamber is heated by four 1200 W band heaters, which are driven by individual PID digital controllers. The chamber is enclosed in a ceramic cover for thermal isolation. Four stainless steel source boats are individually mounted on the tip of stainless steel sheathed thermoresistors, which enable an accurate measurement of the actual evaporation temperature. These rods may slide from the cold side (gas inlet) to the evaporation site at the desired evaporation temperature (see Fig. 1 bottom). The compression fittings in the inlet head allow the movement of the rods avoiding significant vacuum drops. In order to prevent cross contamination, the source boats slide within individual 25 cm long and 12 mm diameter borosilicate glass tubes, through which the Ar carrier gas flows. An Ar bypass flow aids to

4

drag the vapor from the gas inlet to the substrate holder (gas outlet side), and enables a fine tuning of the background pressure. The carrier gas flows are measured by rotameters and adjusted with needle valves. The substrate holder is a copper cylinder, which is cooled down with water pumped from a thermostated reservoir. A thermoresistor is placed between the substrate holder and the substrate enabling an accurate measurement of the substrate temperature.

2.2   PbI$_2$ film deposition conditions

Lead iodide (Sigma-Aldrich 99 % purity) was deposited as purchased by LP-VPD. The source evaporation temperature (T_{evap}), substrate temperature (T_{subs}) and deposition time (t) were varied to evaluate their impact on the film formation. Background pressure was typically between 0.4 and 0.8 mbar. A uniform temperature profile from the inlet to the outlet side of 350, 450, 430 and 400°C was set. These set points were measured inside the chamber at the centre of the band heaters. The Ar flow through the inner tube was fixed at 3 sccm while the bypass flow was kept at 10 sccm. These flows raise the operation pressure between 3.8 and 4.3 mbar.

Commercial glass slides, indium tin oxide (ITO)-coated glass, fluorine doped tin oxide (FTO)-coated glass and FTO-coated glasses with a 15-20 nm dense TiO$_2$ layer were used as substrates. TiO$_2$ was deposited by spray pyrolysis from Titanium diisopropoxide bis (acetylacetonate) 75 wt. % in isopropanol in a 0.2 molar solution followed by an annealing step on a hotplate at a temperature of 550°C in air. The substrates were pre-cleaned with distilled water, isopropyl alcohol and acetone and dried with nitrogen.

Samples preparation conditions and samples names are presented in Table 1. On the one hand, we have used two substrate temperatures, $T_{subs} = 40°C$ and $T_{subs} = 80°C$, which are labeled as cold (C) and hot (H), respectively. On the other hand, two source evaporation temperatures were used in this work, namely $T_{evap} = 310°C$ and $T_{evap} = 350°C$, corresponding to two

5

different evaporation regimes, which we designate as slow (S) and fast (F) evaporation rate, respectively. Finally, the number in the samples label indicates the deposition time t in minutes. As stated above, we designed the experiments bearing in mind that the deposition chamber should be compatible with industrial needs, thus requiring that the system remains as simple as possible to avoid increasing complexity, extra costs and maintenance. As such, the chosen substrate temperatures span the range of achievable temperatures using water as cooling fluid, and therefore avoiding the use of cooling baths or mixtures with alcohols or oils. The chosen evaporation temperature of 310ºC is a practical lower limit, since using lower evaporation temperatures (e.g. <300ºC) would yield too slow evaporation rates, and therefore very slow deposition rates (<10 nm/min) compromising technological interest. On the other hand, the higher evaporation temperature of 350ºC represents a top limit, since using even higher evaporation temperatures would increase dramatically the evaporation rate, and consequently the deposition rate too. This would make it extremely difficult to control the film morphology and its reproducibility.

2.3   Characterization

Scanning electron microscopy (SEM) analyses were carried out by using a focused ion beam (FIB)/SEM dual beam system (FEI Helios 600) at an acceleration voltage of 5 kV. Cross sections of the films were done with a FIB using Ga-Ions with an acceleration voltage of 30 kV. Before carrying out the cross sections, the region of interest was covered with a Pt-layer deposited by Electron Beam Induced Deposition (EBID) (thickness ranging from about 100 nm to 500 nm), hence avoiding damage by imaging or milling with Ga-ions. Above this layer, a second thicker layer of around 1 to 2 μm of Pt is deposited by Ion Beam Induced Deposition (IBID), improving the damage resistance and allowing for preparation of homogeneous cross sections. X-ray diffraction (XRD) patterns were obtained with an X-ray diffractometer (Rigaku SmartLab 3) equipped with a Cu Kα source, working in Bragg−Brentano geometry on a flat sample holder. The XRD pattern acquisition was

performed with 0.02° interval steps in the 2θ range of 5−70°. The average crystallite size was estimated using Scherrer's equation [32].

Normal incidence transmittance T and reflectance R spectroscopy were performed using a spectrophotometer composed of a 2 nm bandwidth reflective diffraction grating monochromator, a filter wheel and an integration sphere. The extinction coefficient k and the absorption coefficient α of the PbI$_2$ films were obtained following the methods described elsewhere [33] and further explained in section 3.3.

Photoluminescence (PL) measurements were made using a Hitachi F-7000 fluorometer equipped with a steady-state Xe lamp as the excitation source. The PL spectra were recorded from 500 to 600 nm with excitation at 350 nm. The slit widths for both excitation and emission were set to yield a spectral resolution of 3 nm.

3   Results and discussion

3.1   Deposition temperatures effect on film properties

Fig. 2 shows SEM images of the surface and cross section of PbI$_2$ films prepared with a deposition time of 10 minutes on glass, at two different evaporation and substrate temperatures. From the bottom to the top of the cross sections images, it is distinguished the glass substrate, the PbI$_2$ film and the Pt protective coating, which is composed of an EBID Pt coating (darkest layer) directly onto the PbI$_2$ film and the thicker IBID Pt layer on top. Samples HS10 and CS10 were obtained at T_{evap} of 310°C, showing hexagonal platelets that grew with hexagonal face width (w_h) around 300-600 nm and thicknesses lower than 50 nm in both samples, suggesting that substrate temperature in the considered range does not influence the platelet size. In turn, sample CF10, obtained at a higher T_{evap} of 350°C and $T_{subs} = 40$°C, has platelets with a wide spread in their size, ranging from $w_h = 0.3$μm to 1.5 μm and thickness around 50 nm, which hints that higher evaporation temperatures can yield larger platelet size. As observed in the SEM top view (Fig. 2), the platelets of sample CF10 have

7

also hexagonal shape, but their corners become rounded. Cross section of HS10 shows a ~280 nm thick compact and uniform PbI_2 layer suggesting that the majority of the platelets grow parallel to the substrate, while few of them crystallize at random angles in relation to the substrate. When decreasing T_{subs} from 80ºC to 40ºC (HS10 to CS10) a greater amount of platelets align vertically to the substrate with various orientations (see Fig. 2). The layer is not as dense as in sample HS10, but the portion of the film composed only of horizontal platelets (that will be called compact layer) has a thickness of ~300 nm, which is very similar to sample HS10. In contrast, when T_{evap} rises to 350ºC (CF10), the platelets grow mostly vertical to the substrate in random orientations and the compact layer reaches a higher thickness of ~450 nm. It is expected that the increased evaporation rate yields a higher deposition rate and thus explains the increase in thickness for equal deposition time. Besides, the SEM images suggest that a higher evaporation rate produces a less ordered arrangement of platelets, resulting in large voids within the films.

Fig. 3 shows top and cross section SEM images of PbI_2 with deposition parameters $T_{subs} = 40$ºC, $T_{evap} = 350$ºC and varying deposition times $t = 5$, 10 and 30 min. The film deposited in 5 min has well defined single platelets, which are mainly hexagonal and are randomly arranged on the substrate. As the deposition time increases to 10 min the platelets begin to lose the hexagonal shape, as stated above, and differ in size. The corresponding cross section image reveals the presence of voids inside the film. Finally, the film deposited after 30 min shows a higher quantity of large clusters that appear as if the hexagons have grown expanding alongside the edges, therefore completely losing the geometrical form. Compared to the samples obtained at shorter deposition times, the crystals have not grown significantly thicker and remain mostly as vertical platelets that leave large voids in the bulk, and therefore, yielding a more porous film.

Thickness values were obtained from cross section images, taking more than 80 points on each image and performing statistical analysis. Table 2 summarizes the mean thickness of the

8

film and the mean thickness of the compact layer (portion with horizontal platelets only) of samples from Fig. 3. Both thicknesses increase with deposition time t, while the relation between compact layer thickness and total film thickness decreases from 67% to 20%. This is produced because, in later stages of film growth, the deposition is dominated by the oblique growth of platelets.

The XRD analysis allows a more general study that enables us to understand the effect of growth on general crystallographic features. Fig. 4 and Fig. 5 show the diffraction patterns corresponding to samples HS10, CS10, CF10 and CF5, CF10, CF30, respectively. In Fig. 4 it is also shown the PbI_2 powder diffractogram as a reference, presenting several diffraction peaks (card number 01-080-1000, ICCD Database). All XRD patterns show reflection peaks at $2\theta = 12.6°$, $25.4°$, $38.6°$ and $52.3°$, which can be associated with (001), (002), (003) and (004) X-ray diffraction planes of hexagonal crystalline structure of PbI_2, respectively (card number 01-080-1000, ICCD Database). For all thin film samples, the lowest angle peak is the most intense, indicating that the preferred hexagonal crystal orientation corresponds to the (001) plane that is perpendicular to the c-axis. This corresponds to platelets aligning horizontally and parallel to the substrate, as seen from the cross section SEM images (Figs. 2 and 3). As thickness is increased and the amount of vertically aligned platelets increase for CF10 and CF30, the peaks corresponding to the basal planes, namely (002), (003) and (004) appear more intense. Other peaks appear in the diffractograms of CF10 and CF30 (marked with * in Fig. 4 and Fig. 5) which can be assigned to the appearance of distorted platelets or clusters as observed from Fig. 3 (CF10 and CF30). In brief, thick films deposited at $T_{subs} = 40°C$ and $T_{evap} = 350°C$ after 10 minutes or more (CF10 and CF30), appear to form two domains, a compact region with horizontally aligned platelets and a top porous zone with randomly aligned vertical platelets and clusters.

Based on Scherrer equation [32], the Full Width at Half Maximum (FWHM) from the main peak, i.e. (001), of the diffraction patterns is inversely proportional to the mean crystal size in

9

the compact layer. In Table 3, the FWHM is compared with average thickness and RMS roughness from cross section images (estimated in a statistical analysis similar to that performed for Table 2). The sample with $T_{subs} = 80°C$ (HS10) has the lowest RMS roughness and also the largest horizontal crystals (smallest FWHM in the dataset). Maintaining a low evaporation temperature ($T_{evap} = 310°C$) and decreasing substrate temperature to $T_{subs} = 40°C$ (CS10) yields films with smaller horizontal crystals, higher average thickness, and increased roughness.

CS10 and CF5 samples show comparable thickness, RMS roughness and FWHM. It appears then that substrate temperature produces a higher impact on crystal and film formation than evaporation temperature. The increase in deposition time at high evaporation rate ($T_{evap} = 350°C$) does not change significantly the platelet size (CF10). Nonetheless, it is observed that the platelets accommodate in orientations different from the substrate plane, yielding larger film roughness. In all samples prepared at $T_{subs} = 40°C$, the roughness represents a 1/3 of average thickness while in the $T_{subs} = 80°C$ sample this relation decreases to 1/4.

3.2 Effect of substrate choice on film properties

In order to understand the influence of the substrate upon film formation we deposited PbI_2 on glass, ITO-coated glass, FTO-coated glass and glass/FTO/TiO_2 substrates. We choose the deposition conditions that produced the most uniform films on glass, namely $T_{subs} = 80°C$, $T_{evap} = 310°C$ and $t = 10$ min (sample HS10). Fig. 6 shows SEM images of surfaces and the cross-sections prepared with FIB of films on different substrates. The glass substrate allows the formation of very compact films. On ITO a compact PbI_2 film grew with a more disordered structure than the same film on glass, and showed a high roughness compared to its average thickness. The XRD pattern of PbI_2/ITO films (Fig. 7) indicates the presence of other orientations besides than (001), but the corresponding peaks intensities are very low

10

compared to the (001) peak, highlighting the dominance of the preferential growth parallel to the substrate. The FWHM values (Table 4) suggest the presence of smaller crystals of PbI_2 onto ITO, which is also observed by SEM images.

The diffractogram of the PbI_2 film deposited on FTO has several reflection peaks with comparable intensities to the peak corresponding to the (001) plane. This aims at a non-preferential growth, as suggested also by the SEM image (Fig. 6 (c)), where the crystals have a wide distribution of orientations. Cross section SEM (Fig. 6 (c)) shows a poor surface coverage and the formation of islands with irregular shapes. These sites can allow the undesirable contact between a possible upper layer and FTO. The PbI_2 film grown on FTO also presents very low average thickness (< 100 nm), implying a lower amount of deposited material in comparison to films grown on other substrates at the same deposition conditions, which indicates a less affinity between PbI_2 vapor and substrate. The higher FWHM (see Table 4) indicates the formation of smaller crystals, as identified also in the surface SEM images.

The addition of a TiO_2 layer between the FTO and the PbI_2 film is frequently used in perovskite solar cells, since the TiO_2 conduction band has a better alignment with that of perovskite than FTO and thus the interface acts as an ohmic contact for electrons [34]. The XRD pattern of $FTO/TiO_2/PbI_2$ evidenced the same peaks and relative intensities than FTO/PbI_2 with the addition of a peak at $2\theta = 43°$, which is related to rutile TiO_2 phase (210) (card number 00-001-1292, ICCD Database). The value of FWHM (see Table 4) suggests that the addition of TiO_2 allows the growth of larger crystals that stack parallel to the substrate leading to the formation of a compact layer with platelets on it. The average thickness of PbI_2 on TiO_2/FTO is comparable to the film grown on glass, indicating that TiO_2 increases the substrate affinity with PbI_2 vapor.

3.3 Optical characterization

The measurements of transmittance T_{meas} and reflectance R_{meas} were made on a PbI$_2$ film grown on quartz, using the same deposition conditions of sample HS10. This sample can be regarded as optically flat (or compact) (see Fig. 2), with a thickness $d = 289$ nm of the compact layer, and very few crystals barely protruding out of it. The index of refraction n (not shown here, available on request) and the extinction coefficient k are involved in the analytical functions for $T(n,k)$ and $R(n,k)$, obtained from a coherent approach of the layer system air/layer/(optically thick substrate). Thus, following the strategy of Denton et al. [33], n and k are obtained by finding the common roots of the two implicit equations $T(n,k)$-$T_{meas} = 0$ and $R(n,k)$-$R_{meas} = 0$, at each measured wavelength value λ. The resulting curve of $k(\lambda)$ leads to the absorption coefficient obtained as $\alpha = 4\pi k/\lambda$. When arranged as a Tauc plot [35], defined by $(\alpha h\upsilon)^2$, where h is Planck's constant and υ is the electromagnetic wave frequency, vs. the photon energy $h\upsilon$, the bandgap energy E_g appears at the photon energy axis intercept. Fig. 8 shows the obtained Tauc plot, where the linear fit (dotted line) yields $E_g = 2.42$ eV ± 0.15 eV from the axis intercept. The error is calculated from statistical error bands derived from the fit. This approximate value of the bandgap encloses literature values of PbI$_2$ films obtained by different deposition methods [17,30]. As a comparison, Fig. 8 shows the data (solid line) obtained by Ahuja et al. using ellipsometry in PbI$_2$ single crystals [31], where the obtained room-temperature bandgap is close to 2.34 eV.

When plotting the data (circles) of $\log(\alpha)$ vs. $h\upsilon$ in a broader range of photon energies, we obtain Fig. 9, that also agrees with the data reported by Ahuja in [31] (solid line). Below the bandgap, the observed linear portion of this curve reveals the presence of energy band-tails, originated from shallow electronic defects. This yields a dependence of the form $\alpha \propto exp(h\upsilon/E_U)$, where E_U is the so-called Urbach energy [36], which is found to be $E_U = 34.7$ meV. Since E_U increases with the defect concentration in the band tails, we notice

that our PbI$_2$ films are not much more defective than the crystals studied in ref.[31], since both curves run nearly parallel below the bandgap. In conclusion the optical characterizations show that, qualitatively, the obtained PbI$_2$ films are consistent with the optical properties of crystalline PbI$_2$, suggesting relatively high purity of the obtained crystallites.

3.4 Room temperature photoluminescence

Room temperature photoluminescent spectra of the PbI$_2$ samples deposited on glass were obtained, as shown in Fig. 10. The PL spectra are highly dependent on the fabrication conditions and hence on the crystallization. Films with similar thickness and RMS, CS10 and CF5 as presented in section 3.1, show similar PL curves. The emission peak at 525 nm is somewhat augmented for the CF5, likely due to the increased amount of the vertically oriented platelets as observed from the SEM images in Figs. 2 and 3. The 525 nm emission peak becomes more intense as the amount of vertically aligned platelets increases, whereas the other two peaks at 550 and 560 nm may correspond to the emission from the horizontally aligned crystal orientation. As the film thickness grows by deposition during 10 and 30 minutes for the T_{evap} = 350°C (CF10 and CF30 samples respectively), the 525 nm signal red shifts into 533 and 537 nm respectively, while the lower energy luminescent signals have minimal contribution and appear as shoulders. The horizontally aligned platelets, despite constituting the thick and dense bottom PbI$_2$ layer that includes a great amount of material and yields a preponderant (001) signal in XRD (see Fig. 5), become buried underneath a growing amount of vertically aligned platelets and their PL signal faints.

Films grown on ITO were also studied and their PL spectrum certainly differs from the films prepared under the same evaporation conditions on glass (see Fig. 11). For ITO, the high energy transition becomes more intense than the lower energy signals and also red shifts; whereas the opposite is observed for films prepared on glass. From the SEM images above, we have established that for films fabricated on ITO, the amount of vertically aligned

13

hexagonal crystals is much higher than for the same films on glass (Fig. 6). This is consistent with the unveiling of the high energy transition, in a similar fashion than in Fig. 10, which becomes stronger for larger amount of vertical platelets.

4   Conclusions

In this work we introduced the low pressure vapor phase deposition method to control the morphology of PbI_2 films grown on different substrates. All the samples have shown a full and uniform coverage of the 2 cm^2 substrates. On the one hand, compact layers with ordered stack of platelets parallel to the glass substrate were obtained at high substrate temperature (80ºC) and low evaporation temperature (310ºC). On the other hand, porous films comprising a bottom compact layer with a disordered arrangement of platelets were deposited on glass at low substrate temperature (40ºC) and high evaporation temperature (350ºC).

Films deposited on ITO- and FTO-coated glasses were rougher than the corresponding film prepared on glass, as seen by a strongly randomized orientation of the platelets. Incorporating a thin TiO_2 layer on FTO allows the formation of a compact layer and larger crystals, suggesting a better affinity between TiO_2 and PbI_2 vapor, than FTO and PbI_2 vapor.

The LP-VPD capability to fine tune the morphology of the PbI_2 thin films has a significant technological impact for the fabrication of optoelectronic devices. For example, porous films should be helpful for the complete reaction of PbI_2 with MAI for obtaining metal organic perovskite for photovoltaic applications. In turn, better electronic transport properties can be obtained from denser PbI_2 films with less disorder which can be beneficial for PbI_2 active layers in X-ray detectors.

14

References

[1]   K.S. Shah, F. Olschner, L.P. Moy, P. Bennett, M. Misra, J. Zhang, M.R. Squillante, J.C. Lund, Lead iodide X-ray detection systems, Nucl. Instrum. Meth. A. 380 (1996) 266–270.

[2]   H. Sun, B. Zhao, D. Yang, P. Wangyang, X. Gao, X. Zhu, Flexible X-ray detector based on sliced lead iodide crystal, Phys. Status Solidi RRL. 11 (2017) 1600397.

[3]   H. Sun, X. Zhu, D. Yang, P. Wangyang, H. Tian, X. Gao, Electrical Behavior of X-Ray Detector Based on PbI_2 Crystal With Coplanar Electrode Structure, IEEE T. Nucl. Sci. 63 (2016) 1790–1796.

[4]   M.A. Green, A. Ho-Baillie, Perovskite Solar Cells: The Birth of a New Era in Photovoltaics, ACS Energy Lett. 2 (2017) 822–830.

[5]   J.-P. Correa-Baena, A. Abate, M. Saliba, W. Tress, T.J. Jacobsson, M. Grätzel, A. Hagfeldt, The rapid evolution of highly efficient perovskite solar cells, Energy Environ. Sci. 10 (2017) 710–727.

[6]   S. Wang, W. Yu, L. Zhang, Y. Yang, Crystallization process of PbI_2 solution in two-step deposition of $CH_3NH_3PbI_3$ for high-performance perovskite solar cells, Sol. Energy Mat. Sol. C. 161 (2017) 444–448.

[7]   M.I. El-Henawey, R.S. Gebhardt, M.M. El-Tonsy, S. Chaudhary, Organic solvent vapor treatment of lead iodide layers in the two-step sequential deposition of $CH_3NH_3PbI_3$-based perovskite solar cells, J. Mater. Chem. A. 4 (2016) 1947–1952.

[8]   G. Pellegrino, S. D'Angelo, I. Deretzis, G.G. Condorelli, E. Smecca, G. Malandrino, A. La Magna, A. Alberti, From PbI_2 to $MAPbI_3$ through layered intermediates, J. Phys. Chem. C. 120 (2016) 19768–19777.

[9]   J. Burschka, N. Pellet, S.-J. Moon, R. Humphry-Baker, P. Gao, M.K. Nazeeruddin, M. Grätzel, Sequential deposition as a route to high-performance perovskite-sensitized solar cells, Nature. 499 (2013) 316–319.

[10]   H. Hu, D. Wang, Y. Zhou, J. Zhang, S. Lv, S. Pang, X. Chen, Z. Liu, N.P. Padture, G. Cui, Vapour-based processing of hole-conductor-free $CH_3NH_3PbI_3$ perovskite/C_{60} fullerene planar solar cells, RSC Adv. 4 (2014) 28964–28967.

[11]   F. Fu, L. Kranz, S. Yoon, J. Löckinger, T. Jäger, J. Perrenoud, T. Feurer, C. Gretener, S. Buecheler, A.N. Tiwari, Controlled growth of PbI_2 nanoplates for rapid preparation of $CH_3NH_3PbI_3$ in planar perovskite solar cells, Phys. Status Solidi A. 212 (2015) 2708–2717.

[12]   G. Chai, S. Wang, Z. Xia, S. Luo, C. Teng, T. Yang, Z. Nie, Tiejun Meng, H. Zhou, PbI 2 platelets for inverted planar organolead Halide Perovskite solar cells via ultrasonic spray deposition, Semicond. Sci. Technol. 32 (2017) 074003.

[13]   Z. Xiao, C. Bi, Y. Shao, Q. Dong, Q. Wang, Y. Yuan, C. Wang, Y. Gao, J. Huang, Efficient, high yield perovskite photovoltaic devices grown by interdiffusion of solution-processed precursor stacking layers, Energy Environ. Sci. 7 (2014) 2619–2623.

[14]   K. Liang, D.B. Mitzi, M.T. Prikas, Synthesis and characterization of organic−inorganic perovskite thin films prepared using a versatile two-step dipping technique, Chem. Mater. 10 (1998) 403–411.

[15]   J.F. Condeles, T.M. Martins, T.C. dos Santos, C.A. Brunello, M. Mulato, J.M. Rosolen, Fabrication and characterization of thin films of PbI_2 for medical imaging, J. Non-Cryst. Solids. 338 (2004) 81–85.

[16]   J. Tonn, A.N. Danilewsky, A. Cröll, M. Matuchova, J. Maixner, Czochralski growth of lead iodide single crystals: Investigations and comparison with the Bridgman method, J. Cryst. Growth. 318 (2011) 558–562.

[17]   İ.A. Kariper, Optical and structural properties of PbI_2 thin film produced via chemical dipping method, Opt Rev. 23 (2016) 401–408.

[18]   M. Zhong, S. Zhang, L. Huang, J. You, Z. Wei, X. Liu, J. Li, Large-scale 2D PbI_2 monolayers: experimental realization and their indirect band-gap related properties, Nanoscale. 9 (2017) 3736–3741.

[19]   M. Baldo, M. Deutsch, P. Burrows, H. Gossenberger, M. Gerstenberg, V. Ban, S. Forrest, Organic Vapor Phase Deposition, Adv. Mater. 10 (1998) 1505–1514.

[20]   P.E. Burrows, S.R. Forrest, L.S. Sapochak, J. Schwartz, P. Fenter, T. Buma, V.S. Ban, J.L. Forrest, Organic vapor phase deposition: a new method for the growth of organic thin films with large optical non-linearities, J. Cryst. Growth. 156 (1995) 91–98.

[21]   F. Yang, M. Shtein, S.R. Forrest, Controlled growth of a molecular bulk heterojunction photovoltaic cell, Nat. Mater. 4 (2005) 37–41.

[22]   M. Rusu, J. Gasiorowski, S. Wiesner, N. Meyer, M. Heuken, K. Fostiropoulos, M.C. Lux-Steiner, Fine tailored interpenetrating donor–acceptor morphology by OVPD for organic solar cells, Thin Solid Films. 516 (2008) 7160–7166.

[23]   C. Rolin, K. Vasseur, J. Genoe, P. Heremans, Growth of pentacene thin films by in-line organic vapor phase deposition, Org. Electro. 11 (2010) 100–108.

[24]   R.R. Lunt, B.E. Lassiter, J.B. Benziger, S.R. Forrest, Organic vapor phase deposition for the growth of large area organic electronic devices, Appl. Phys. Lett. 95 (2009) 233305.

[25]   D. Liu, J. Yang, T.L. Kelly, Compact Layer Free Perovskite Solar Cells with 13.5% Efficiency, J. Am. Chem. Soc. 136 (2014) 17116–17122.

[26]   J.H. Heo, H.J. Han, D. Kim, T.K. Ahn, S.H. Im, Hysteresis-less inverted $CH_3NH_3PbI_3$ planar perovskite hybrid solar cells with 18.1% power conversion efficiency, Energy Environ. Sci. 8 (2015) 1602–1608.

[27]   L. Huang, X. Sun, C. Li, R. Xu, J. Xu, Y. Du, Y. Wu, J. Ni, H. Cai, J. Li, Z. Hu, J. Zhang, Electron transport layer-free planar perovskite solar cells: Further performance enhancement perspective from device simulation, Sol. Energy Mat. Sol. C. 157 (2016) 1038–1047.

[28]   G. Zentai, L. Partain, R. Pavlyuchkova, C. Proano, G.F. Virshup, P. Bennett, K. Shah, Y. Dmitriev, J. Thomas, Improved properties of PbI_2 x-ray imagers with tighter process control and using positive bias voltage, in: Proc. SPIE 5368, Medical Imaging 2004: Physics of Medical Imaging, (2004), 668–676.

[29]   I. Levine, S. Gupta, T.M. Brenner, D. Azulay, O. Millo, G. Hodes, D. Cahen, I. Balberg, Mobility–Lifetime Products in $MAPbI_3$ Films, J. Phys. Chem. Lett. 7 (2016) 5219–5226.

[30]   T. Ghosh, S. Bandyopadhyay, K.K. Roy, S. Kar, A.K. Lahiri, A.K. Maiti, K. Goswami, Optical and structural properties of lead iodide thin films prepared by vacuum evaporation method, Cryst. Res. Technol. 43 (2008) 959–963.

[31]   R. Ahuja, H. Arwin, A. Ferreira da Silva, C. Persson, J.M. Osorio-Guillén, J. Souza de Almeida, C. Moyses Araujo, E. Veje, N. Veissid, C.Y. An, I. Pepe, B. Johansson, Electronic and optical properties of lead iodide, J. Appl. Phys. 92 (2002) 7219–7224.

[32]   T. Chung, S. Kim, S. Bae, S.-W. Lee, K. Cho, S. Lee, Y. Kang, H.-S. Lee, D. Kim, Characterization of methylammonium lead iodide perovskite solar cells by surface morphology changes, J. Nanosci. Nanotechno. 17 (2017) 4817–4821.

[33]   R.E. Denton, R.D. Campbell, S.G. Tomlin, The determination of the optical constants of thin films from measurements of reflectance and transmittance at normal incidence, J. Phys. D: Appl. Phys. 5 (1972) 852.

[34]   W. Yan, S. Ye, Y. Li, W. Sun, H. Rao, Z. Liu, Z. Bian, C. Huang, Hole-Transporting Materials in Inverted Planar Perovskite Solar Cells, Adv. Energy Mater. 6 (2016) 1600474.

[35]   D.K. Schroder, Semiconductor Material and Device Characterization, third ed., John

18

Wiley and Sons, Hoboken, New Jersey, 2006.

[36]   J.I. Pankove, Optical Processes in Semiconductors, second ed., Dover Publications, New York, 1975.

List of tables captions

Table 1. Summary of samples labels and deposition conditions.

Table 2. Measured parameters from SEM images of cross sections of samples obtained varying deposition time with $T_{subs} = 40°C$ and $T_{evap} = 350°C$.

Table 3. Quantification of average thickness and RMS roughness from cross-section SEM images and Full Width at Half Maximum (FWHM) from X-ray diffraction, of samples on glass varying source evaporation temperature, substrate temperature and deposition time.

Table 4. Quantification of average thickness from cross-section SEM images and Full Width at Half Maximum (FWHM) from X-ray diffraction, of PbI_2 grown on glass, ITO, FTO and FTO/TiO2.

List of figures captions

Fig. 1. Schemes of LP-VPD chamber and temperature gradient inside the chamber. See text for detailed descriptions.

Fig. 2. (left) Surface SEM images of PbI_2 films deposited on glass substrates and (right) their corresponding cross section prepared with FIB. Deposition time was fixed at 10 minutes, while substrate temperature (T_{subs}) varies between 40 and 80°C and source evaporation temperature (T_{evap}) varies between 310 and 350°C, as indicated in the labels. The 1 µm and 5 µm scale bars apply to images in the left and right columns, respectively. The cross section images were obtained at a tilt angle of 52°. In the top cross section is identified as a reference for all samples the EBID and IBID Pt protective coatings.

Fig. 3. (left) Surface SEM images and (right) their corresponding cross-section of PbI_2 films on glass with a substrate temperature of 40°C and source evaporation temperature of 350°C. Deposition times (t) are 5 (CF5), 10 (CF10) and 30 (CF30) minutes as shown in the figure. The images of cross sections were obtained at a tilt angle of 52°.

Fig. 4. X-ray diffraction patterns of PbI_2 samples as powder and as thin films deposited on glass varying source evaporation temperature (T_{evap}), substrate temperature (T_{subs}) with fixed deposition time $t = 10$ min. Peaks other than (001), (002), (003) and (004) are marked with *.

Fig. 5. X-ray diffraction patterns of PbI_2 samples on glass varying the deposition time, as indicated in the labels, fixing source evaporation temperature $T_{evap} = 310°C$, and substrate temperature $T_{subs} = 40°C$. Peaks other than (001), (002), (003) and (004) are marked with *.

Fig. 6. SEM images of surface and cross-section of PbI_2 grown on glass (HS10) (a), ITO (b), FTO (c) and TiO_2 covered FTO substrates (d). Deposition parameters were fixed as follow: $T_{evap} = 310°C$, $T_{subs} = 80°C$ and $t = 10$ min. Images of cross sections were taken at a sample tilt of 52°.

Fig. 7. X-ray diffraction patterns of PbI_2 samples on glass (HS10), ITO, FTO and TiO_2 covered FTO substrates. Deposition parameters were fixed as follow: $T_{evap} = 310°C$, $T_{subs} = 80°C$ and deposition time 10 minutes. Identified diffraction peaks from ICCD database were taken from cards 01-080-1000, 01-077-0452, 00-001-1292 and 00-006-0416 for PbI_2, FTO,

TiO$_2$ and ITO respectively. Diffraction peaks were marked with °, +, × and ♦ for PbI$_2$, FTO, TiO$_2$ and ITO, respectively.

Fig. 8. Tauc plot of PbI$_2$ film grown on quartz (data represented with open circles), showing the bandgap value at the axis intercept (linear fit shown by the dashed line). Data from reference [31] (solid line) are also presented for comparison.

Fig. 9. Dependence of log(α) vs. photon energy for PbI$_2$ film grown on quartz (data represented with open circles). Data from reference [31] (solid line) are also presented for comparison. Below the gap, a linear dependence is shown by the dashed line, yielding the Urbach energy (see text for details).

Fig. 10. Room temperature photoluminescent (PL) spectra of PbI$_2$ films grown on glass, varying source evaporation temperature (T_{evap}) and deposition time (t). Substrate temperature was fixed to 40°C.

Fig. 11. Room temperature photoluminescent (PL) spectra of PbI$_2$ films grown on glass (HS10) and ITO. Deposition parameters were fixed as follow: T_{evap} = 310°C, T_{subs} = 80°C and deposition time (t) 10 minutes.

Tables

Table 1.

Name	Substrate	T_{subs} [°C]	T_{evap} [°C]	t [min]
HS10	Glass	80	310	10
CS10	Glass	40	310	10
CF5	Glass	40	350	5
CF10	Glass	40	350	10
CF30	Glass	40	350	30
ITO	ITO	80	310	10
FTO	FTO	80	310	10
FTO/TiO$_2$	FTO/TiO$_2$	80	310	10

Table 2.

Deposition time [min]	Thickness [nm]		Compact thickness/film thickness
	Compact layer	Film	
5	205	305	0.67
10	451	1 670	0.27
30	1 043	5 117	0.20

Table 3.

Sample name	Average thickness [nm]	RMS roughness [nm]	FWHM (001)
HS10	320	86	0.064
CS10	380	149	0.101
CF10	1 005	368	0.087
CF5	319	133	0.090

Table 4.

Substrate	Average thickness [nm]	FWHM (001)
Glass	320	0.064
ITO	241	0.143
FTO	96	0.216
FTO/TiO2	208	0.141

22

Highlights

- PbI$_2$ films are prepared by low pressure vapor phase method

- Homogeneous films are obtained on insulating and conducting substrates

- Dense and porous films can be obtained varying deposition temperatures
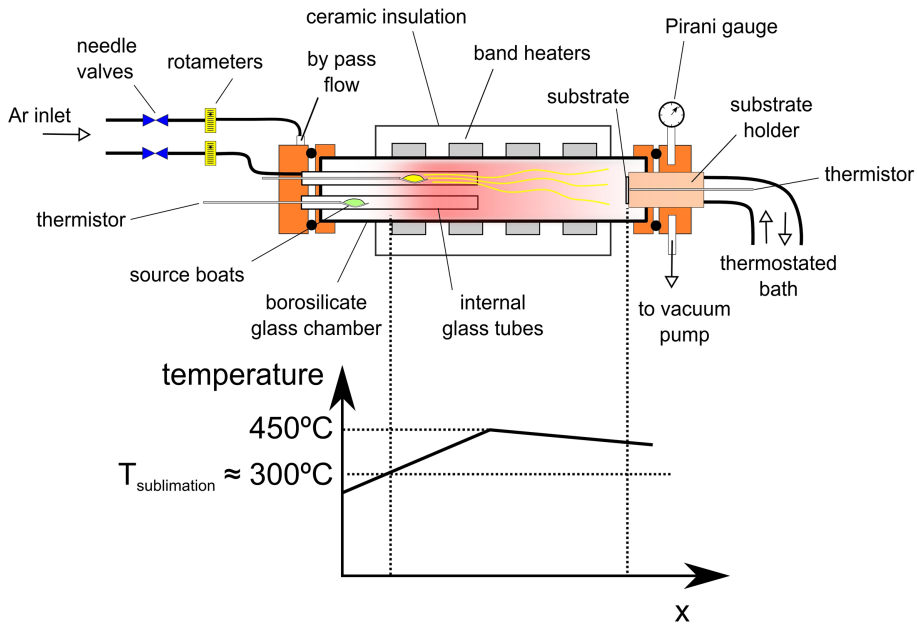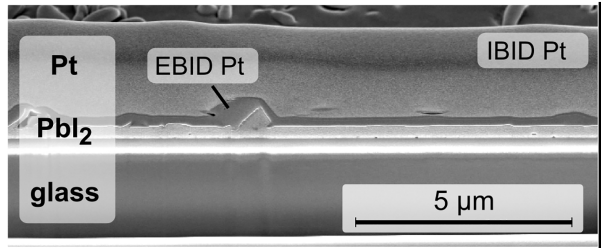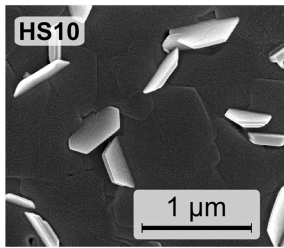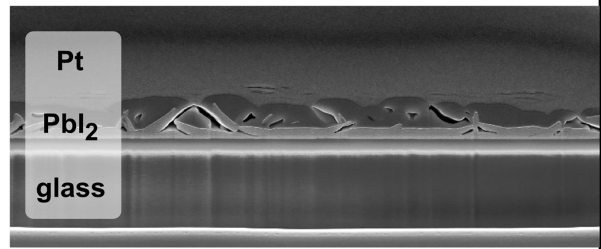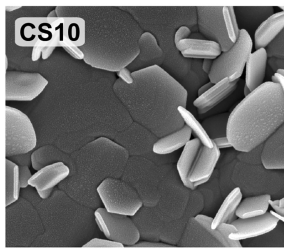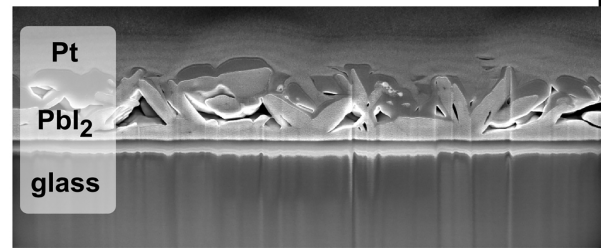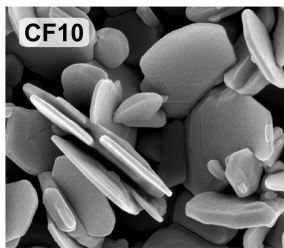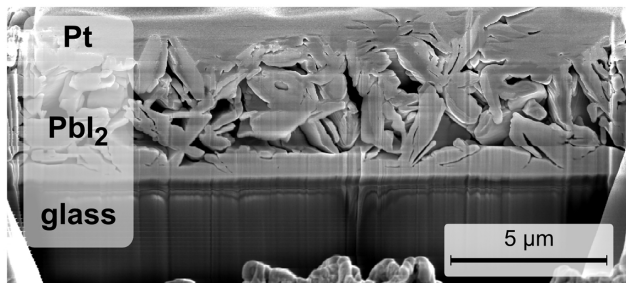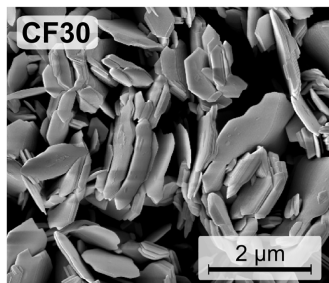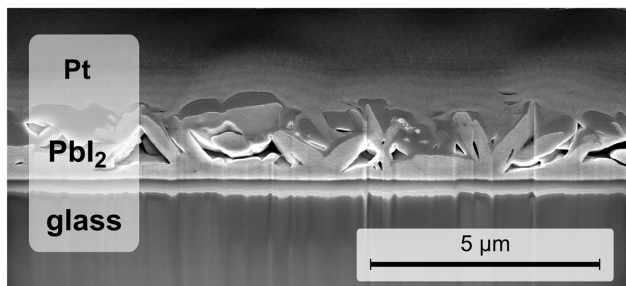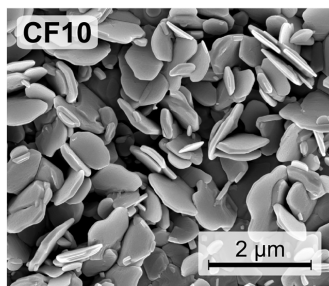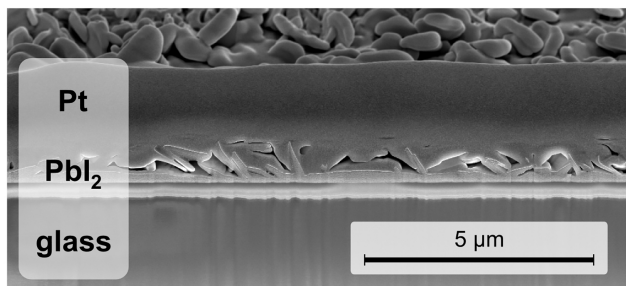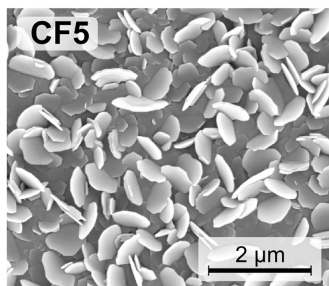
Figure 1
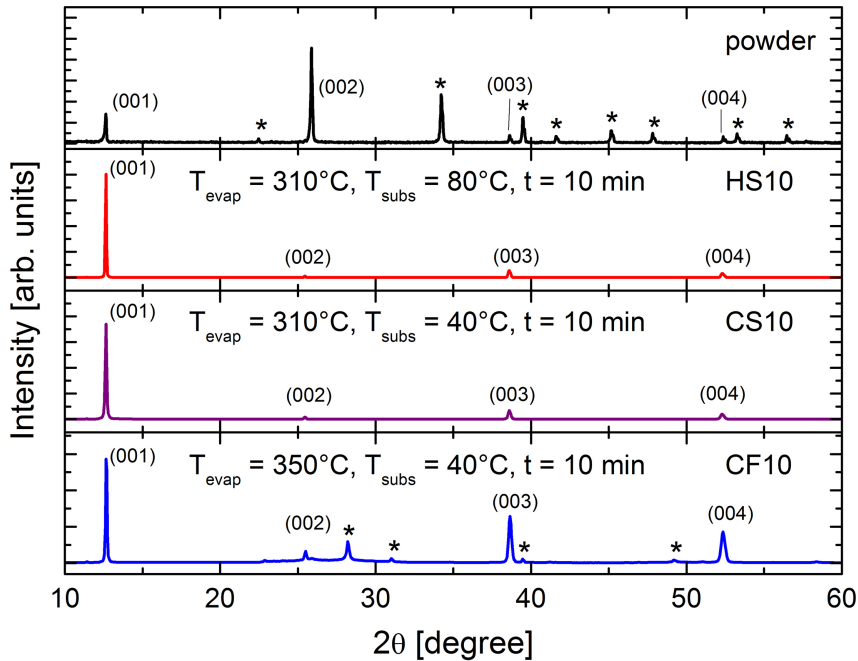
Figure 2
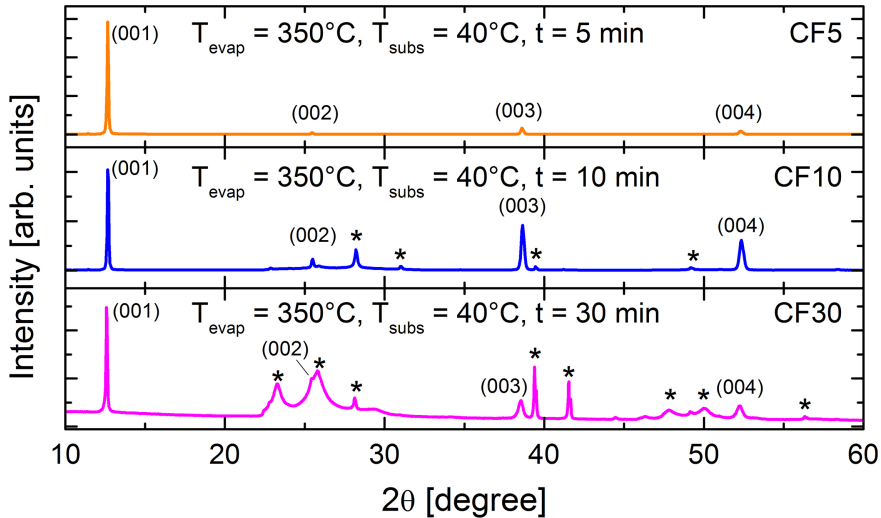
Figure 3

Figure 4

Figure 5
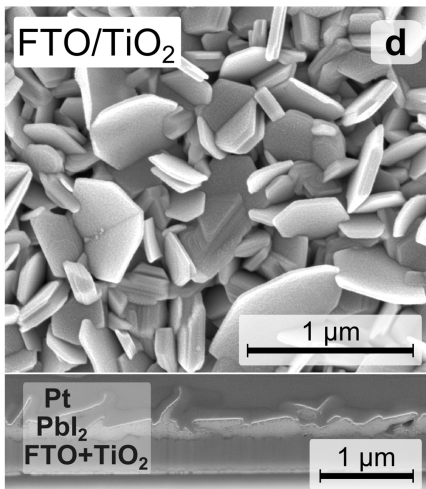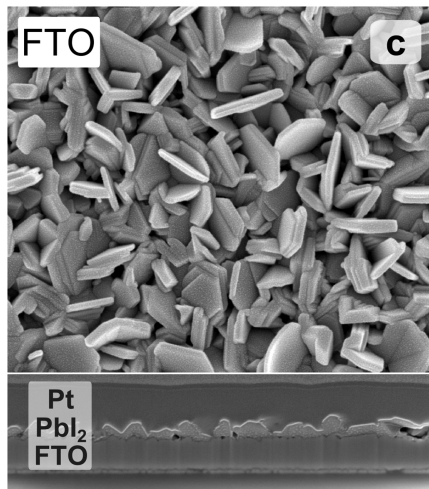
Figure 6

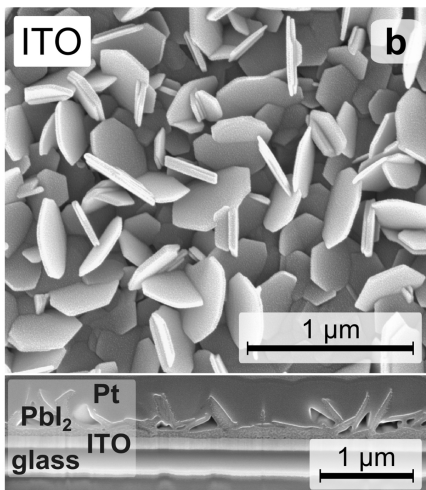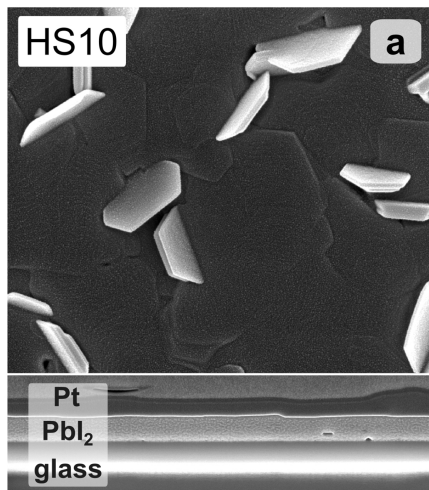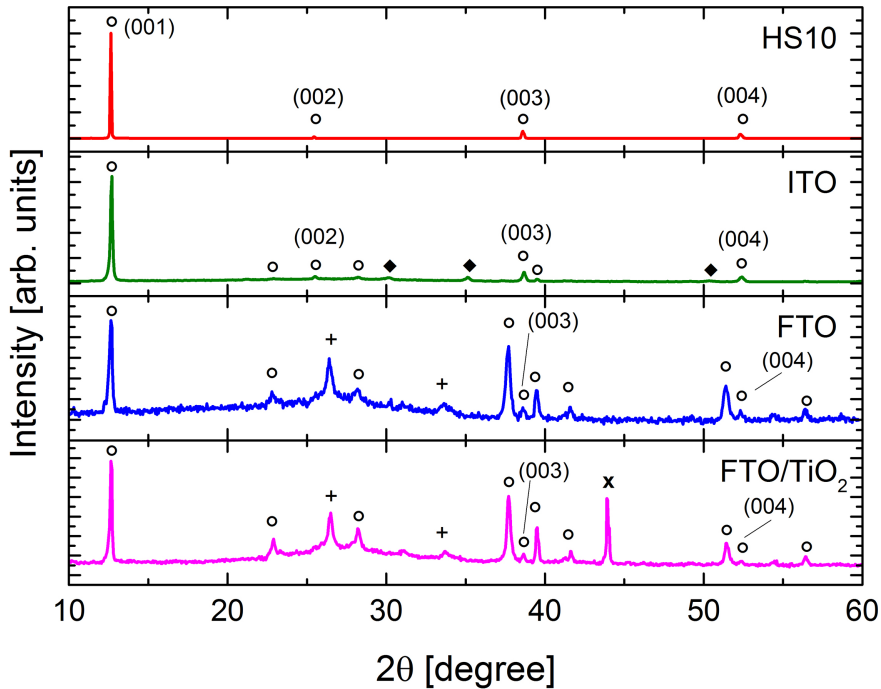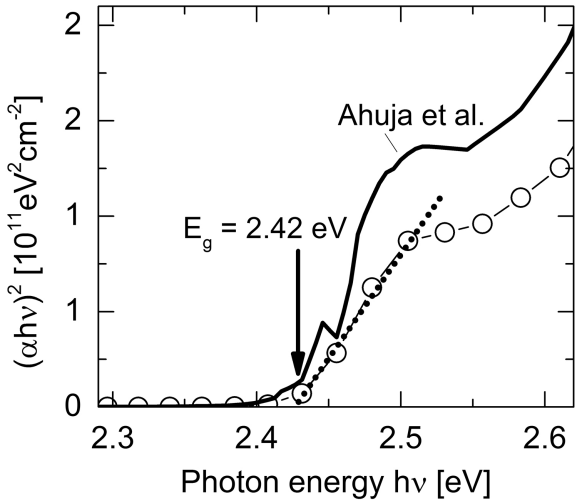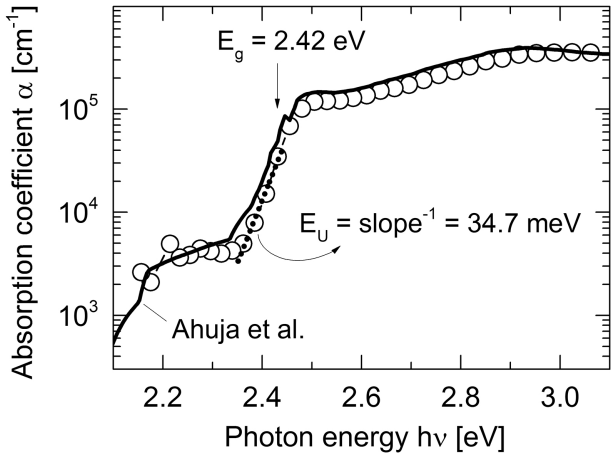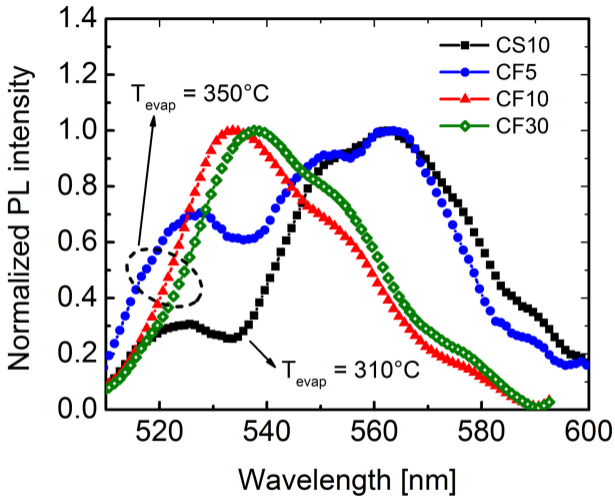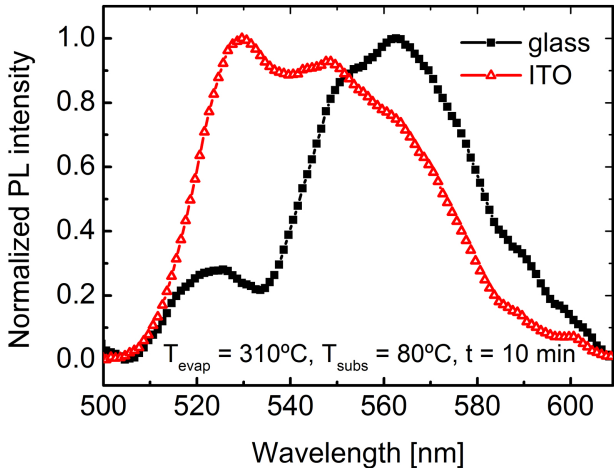Figure 7

Figure 8

Figure 9

Figure 10

T_{evap} = 310ºC, T_{subs} = 80ºC, t = 10 min

Figure 11